Induction of caspase-mediated apoptosis in HepG2 liver carcinoma cells using mutagen-antioxidant conjugated self-assembled novel carbazole nanoparticles and in silico modeling studies

Journal:	*ACS Omega*
Manuscript ID	ao-2020-04461n.R1
Manuscript Type:	Article
Date Submitted by the Author:	28-Oct-2020
Complete List of Authors:	Anand, Krishnan ; University of the Free State, Department of Chemical Pathology, Sheik Abdul, Naeem ; University of KwaZulu-Natal, Discipline of Medical Biochemistry, Ghazi, Terisha ; University of KwaZulu-Natal, Discipline of Medical Biochemistry, Ramesh, Muthusamy; National Institute of Pharmaceutical Education and Research, Department of Medicinal Chemistry Gupta, Gaurav ; Suresh Gyan Vihar University Tambuwala, Murtaza; University of Ulster, Pharmacy DUREJA, HARISH; M.D. UNIVERSITY, ROHTAK, DEPARTMENT OF PHARMACEUTICAL SCIENCES Singh, Sachin Kumar; Lovely Professional University Faculty of Applied Medical Sciences, Pharmacy Chellappan, Dinesh; International Medical University, School of Pharmacy Dua, Kamal ; University of Technology Sydney Pandi, Boomi ; Alagappa University Saravanan, Muthupandian; Mekelle University College of Health Sciences, Department of Medical Microbiology and Immunology Chuturgoon, Anil; University of KwaZulu-Natal,

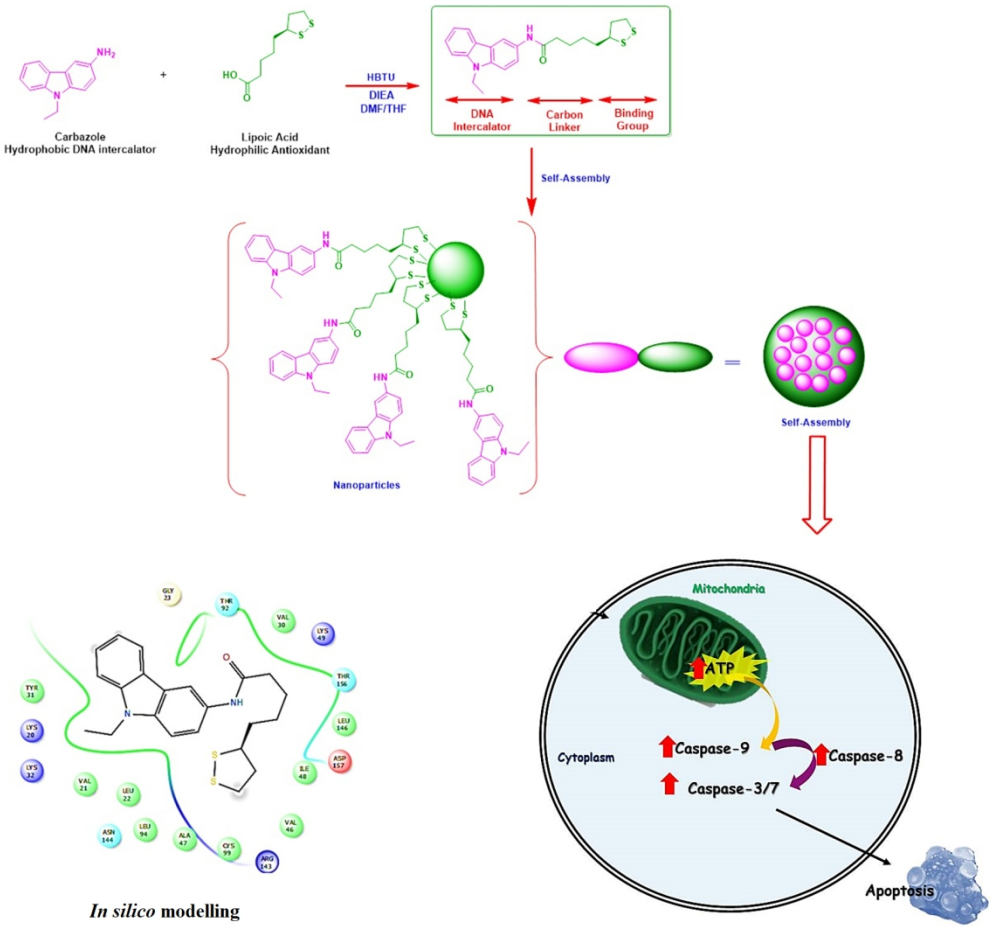

480x457mm (96 x 96 DPI)

Induction of caspase-mediated apoptosis in HepG2 liver carcinoma cells using mutagen-antioxidant conjugated self-assembled novel carbazole nanoparticles and *in silico* modeling studies

Krishnan Anand[a]*, Naeem Sheik Abdul[b], Terisha Ghazi[b], Muthusamy Ramesh[c], Gaurav Gupta[d], Murtaza M Tambuwala[e], Harish Dureja[f], Sachin Kumar Singh[g], Dinesh Kumar Chellappan[h], Kamal Dua[i,j,k], Boomi Pandi[l], Muthupandian Saravanan[m]*, Anil Amichund Chuturgoon[b]*

[a]Department of Chemical Pathology, School of Pathology, Faculty of Health Sciences and National Health Laboratory Service, University of the Free State, Bloemfontein, South Africa

[b]Discipline of Medical Biochemistry, School of Laboratory Medicine and Medical Science, University of KwaZulu-Natal, South Africa

[c]Department of Pharmaceutical Analysis, Omega College of Pharmacy, Hyderabad 501 301, India

[d]School of Pharmacy, Suresh Gyan Vihar University, Jagatpura Mahal Road, 302017, Jaipur, India

[e]School of Pharmacy and Pharmaceutical Science, Ulster University, Coleraine, County Londonderry, BT52 1SA, Northern Ireland, United Kingdom; School of Biomedical Sciences, University of Ulster, Coleraine, BT52 1SA, Northern Ireland, United Kingdom

[f]Department of Pharmaceutical Sciences, Maharshi Dayanand University, Rohtak, 124001, Haryana, India

[g]School of Pharmaceutical Sciences, Lovely Professional University, Phagwara, Punjab, 144411, India

[h]School of Pharmacy, International Medical University, Bukit Jalil, 57000, Kuala Lumpur, Malaysia

[i]Discipline of Pharmacy, Graduate School of Health, University of Technology Sydney, Ultimo, NSW, 2007, Australia

[j]Priority Research Centre for Healthy Lungs, Hunter Medical Research Institute (HMRI) & School of Biomedical Sciences and Pharmacy, The University of Newcastle (UoN), Callaghan, NSW, 2308, Australia

[k]School of Pharmaceutical Sciences, Shoolini University of Biotechnology and Management Sciences, Solan, 173229, India

[l]Department of Bioinformatics, Alagappa University, Karaikudi, 630 003, India

[m]Department of Microbiology and Immunology, Division of Biomedical Sciences, School of Medicine, College of Health Sciences, Mekelle University, Mekelle -1871, Ethiopia

***Corresponding authors**.

*Krishnan Anand, (T:+27632430012; E-mail organicanand@gmail.com)

[*]Muthupandian Saravanan, (Tel:+251344416690; E-Mail: saravanan.muthupandian@mu.edu.et)

[*]Anil Amichund Chuturgoon, (Tel +27312604404; E-mail: chutur@ukzn.ac.za)

Abstract

In this study, the novel self-assembled carbazole-thiooctanoic acid nanoparticles (CTN) were synthesized from amino carbazole (a mutagen), and thiooctanoic acid (an antioxidant). The nanoparticles were characterized by hyperspectral techniques. Then, the antiproliferative potential of CTN was determined in HepG2 liver carcinoma cells. The study employed a solvent-antisolvent interaction method to synthesize a spherical CTN of size less than 50 nm. Moreover, carbazole-thiooctanoic acid (CT) was subsequently capped to gold nanoparticles (AuNPs) in the additional comparative studies. The CT derivative was synthesized from carbazole, and lipoic acid by amide bond formation reaction using coupling agent. Further, it was characterized by IR, ^{1}H-NMR, DLS, and TEM techniques. The carbazole-thiooctanoic acid capped gold nanoparticles (CTAuNPs) was prepared from CT, chloroauric acid, and $NaBH_4$. The CTAuNPs were characterized by UV–Vis, HRTEM, DLS, and FTIR techniques. The cytotoxicity and apoptosis-inducing ability of both nanoparticles were determined in HepG2 cells. The results demonstrate that CTN possess antiproliferative activity in the cancerous HepG2 cells. Moreover, molecular docking and molecular dynamics studies were conducted to explore the therapeutic potential of CT against human EGFR suppressor protein to gain more insights into the binding mode of the CT, which may show a significant role in anticancer therapy.

Keywords: self-assembly; CTAuNPs; amino carbazole; lipoic acid; amphiphile; HepG2 cells; apoptosis, EGFR

1. Introduction

Chemotherapeutic agents play a vital role in the treatment of cancer. Amongst them, carbazoles (a model DNA intercalator), and its derivatives have potential biological activities[1]. The enhanced cellular internalization of carbazole and its reduced toxicity to normal cells are significant in biological studies. In the recent past, nanodrug-based strategies are widely used to combat multidrug resistance (MDR)[2]. The enhanced permeability and retention (EPR) effect of self-assembled nanoparticles has garnered significant interest in drug delivery. A compound that combines two different drugs in one molecule has shown a synergistic effect in the treatment of diseases, and it can produce enhanced pharmacological effects. Such compounds are referred to as twin drugs and often show two different pharmacological activities in cancer cells[3]. Although several metals are used for nano synthesis, gold (inert metal) is preferred in medicine because of its low toxicity in healthy human cells. In general, antibodies and targeting moieties are conjugated by adsorption to the gold surface. A drawback of surface adsorption is the susceptibility of proteins to denaturation and in some cases limited ligand interactions with cell surface targets due to steric hindrance[4]. The capping of organic ligands such as amines, thiols[5], dithiols, etc adds stability to gold nanoparticles. The interaction between ligand and the nanometal have been investigated earlier[6]. Dithiol ligands were conjugated to gold nanoparticles by sulfur ends[7]. The organic-capping layer formed duringmetal-ligand interactions plays a vital role in high-performance biomaterials[8]. Lipoic acid (LA) is a vitamin-like bioactive small molecule called antioxidant. The antioxidant important therapeutic potential in conditions where oxidative stress (ROS) is involved. It is sulphur-rich compound found in cruciterous vegetables like broccoli and cabbage[9].

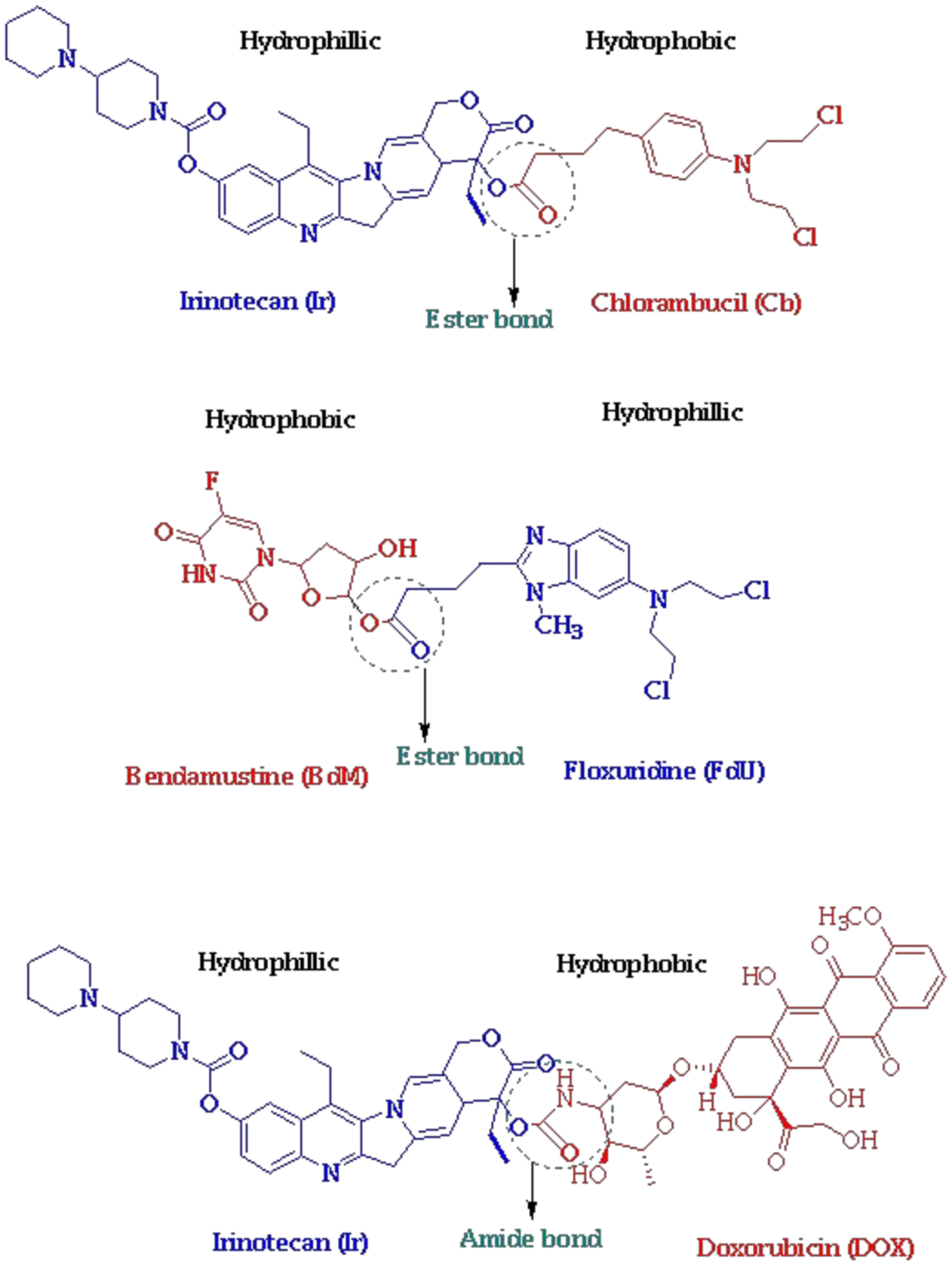

Figure 1. The literature reported amphiphilic Drug–Drug conjugate for cancer therapy

Nano drugs self assembled delivery systems are the most important for cancer chemotherapy and it is considered a better method because of their stability in the bloodstream, high drug loading and controllable release from carriers at target sites[10]. Moreover, this strategy can improve the efficiency of cellular uptake because of their ability to enhance drug delivery efficacy and reduce drug side effects. Different amphiphilic drug-drug conjugate have been

made using dissimilar of hydrophobic and hydrophilic drugs (Fig. 1). The resulting amphiphilic twin drugs could self-assemble into nanoparticles with high drug loading and improve cancer therapeutic efficacy. For example, irinotecan as hydrophilic anticancer drug and chlorambucil hydrophobic anticancer drug were conjugated through the hydrolyzable ester linkage[11]. The amphiphilic nanoparticles were composed of two drug-drug conjugates, including doxorubicin (DOX)-chlorambucil (Cb) and irinotecan (Ir)-Cb conjugates. Floxuridine (FdU) as hydrophilic anticancer drug was tethered with hydrophobic anticancer drug of bendamustine (BdM) to form amphiphilic twin drug[12]. The twin drug molecules interconnected by an ester bond or amide bond could readily self-assemble into stable and uniform nanoparticles. The nanoparticles can be delivered to the action sites of a body via physical entrapment or chemical conjugation, better therapeutic efficacy against tumors and without side effects over free drugs. More importantly, after uptake by tumor cells and chemoenzymatic activity, the conjugates could be easily disintegrated into individual free drugs and it can induce nonoverlapping but synergistic pharmacological effects and simultaneously improve the therapeutic efficacy in vitro. Direct conjugation of hydrophobic drug and small organic compounds is recently established as a new nano-drug delivery system. Due to a wide variety of therapeutic applications, nitrogen-containing heterocycles hold its significancein medicine[13], and carbazole derivatives are one such example. The thiooctanoic acid (lipoic acid) belongs to the family of tocopherols and tocotrienols. The mutagen-amino carbazole (AC) and antioxidant-lipoic acid (LA) are the unique compounds; they are expected to excel for cancer therapeutic applications and may be suitable candidates to solve the drawbacks. The present study chose the hydrophobic amino carbazole (AC) and hydrophilic lipoic acid (LA) for synergistic combination in chemotherapy. Moreover, carbazole thiooctanoic acid (CT) functionalized gold nanoparticles were synthesized. The newly synthesized carbazole self-assembled nanoparticles and conjugated gold nanoparticles were evaluated for their antiproliferative activities against HepG2 cells. The amphiphilic self-assembled nanoparticles (CTN) increased the activity of the extrinsic caspase 8, intrinsic caspase 9 and executioner caspases and LDH release was not altered significantly suggesting apoptosis instead of necrosis. Furthermore, the molecular docking and molecular dynamics of mono CT molecule to EGFR were performed, to explore the other possible target.

2. Results and Discussion

The compound carbazole thiooctanoic acid (CT) [**3**] was synthesized by reacting 3-amino-9-ethyl carbazole (AC) [**1**] and lipoic acid (LA) [**2**] in the presence of HBTU and DIEA. The base deprotonates the carboxylic acid. The resulting carboxylate anion attacks the electron-deficient carbon atom of HBTU (Fig. 2). The resulting HOBt anion reacts with the newly formed activated carboxylic acid derived intermediate to form an OBt activated ester. The amine reacts with the OBt activated ester to form the amide product amphiphilic CT.

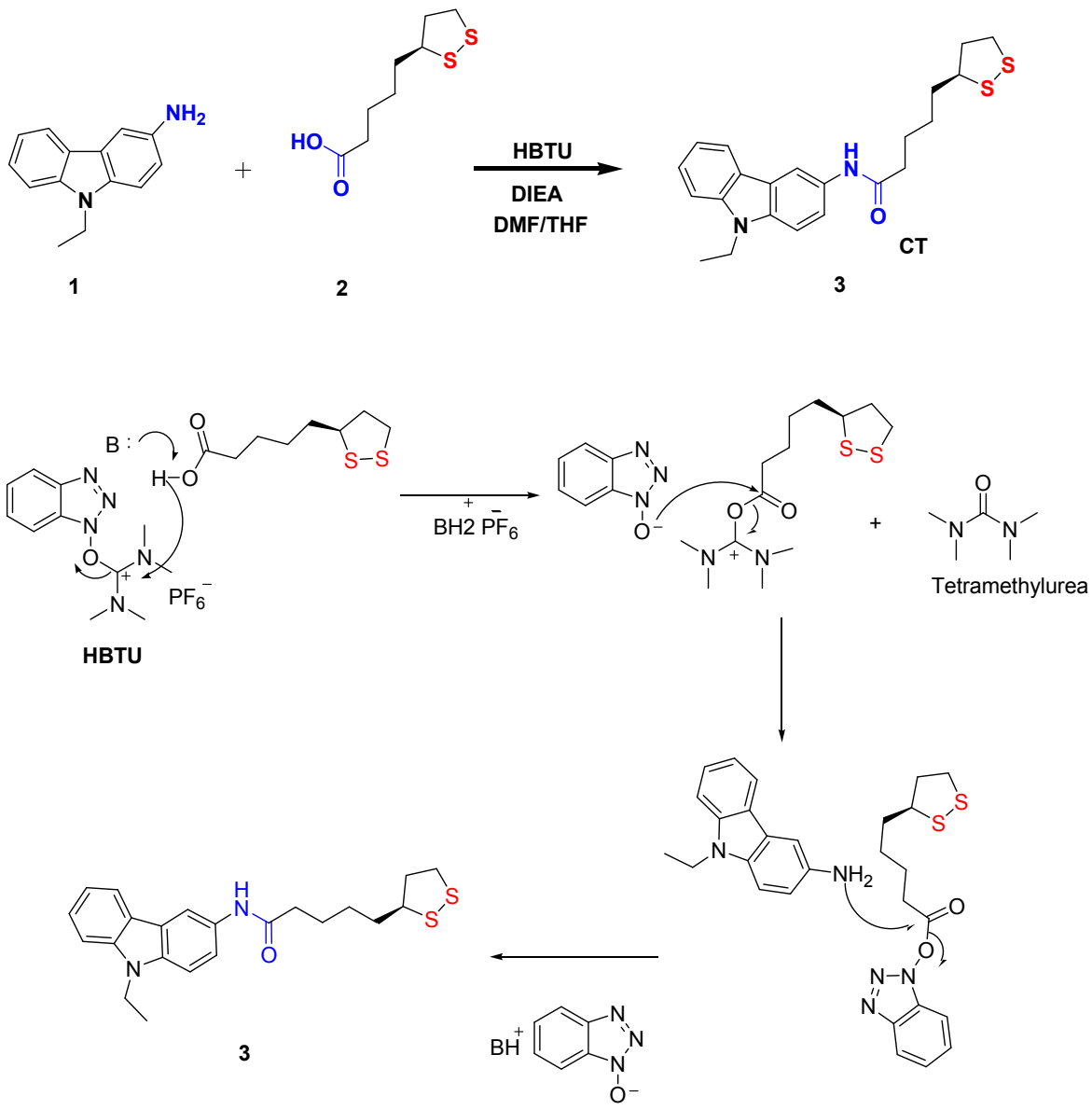

Figure 2 Synthesis of carbazole thiooctanoic acid (CT) [**3**] and Plausible ‘’amine to amide’’ mechanism for the formation of CT

Lipoic acid is a water-soluble antioxidant and amino carbazole is a water-insoluble DNA intercalator. Therefore, the resultant CT molecule is amphiphilic and self-assembles to form nanoparticles in an aqueous environment, a benefit derived from the amphiphilic nature (Fig. 3). The dialysis method was employed to prepare the self-assembled CT twin drug nanoparticles. The acetone solution of CT was added with deionized water and dialyzed to remove the acetone, thereby a stable nanoparticle solution was obtained with 0.5 mg/mL concentration.

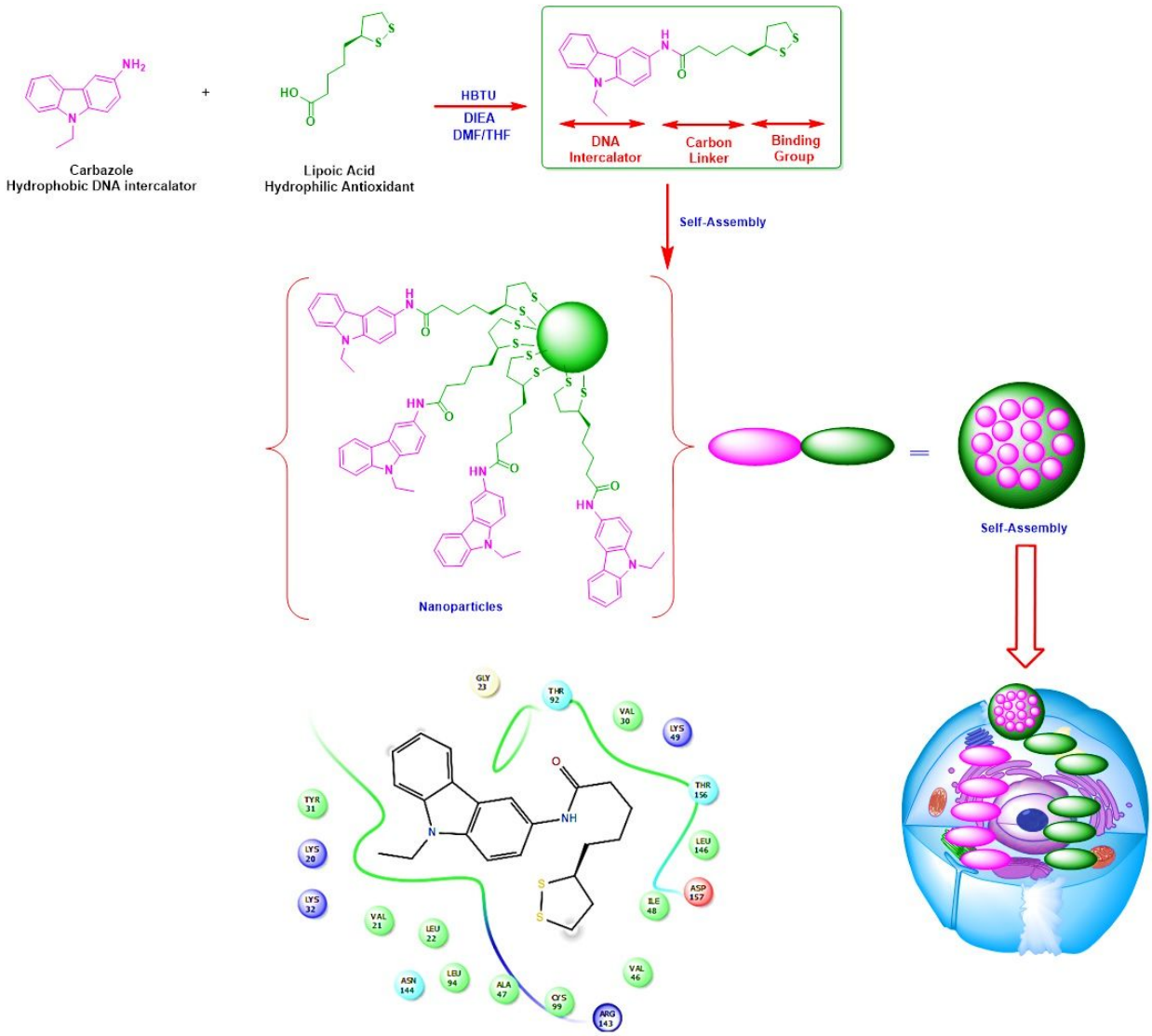

Figure 3 Schematic route for the formation of amphiphilic twin bioactive molecule and its self-assembly for endocytosis.

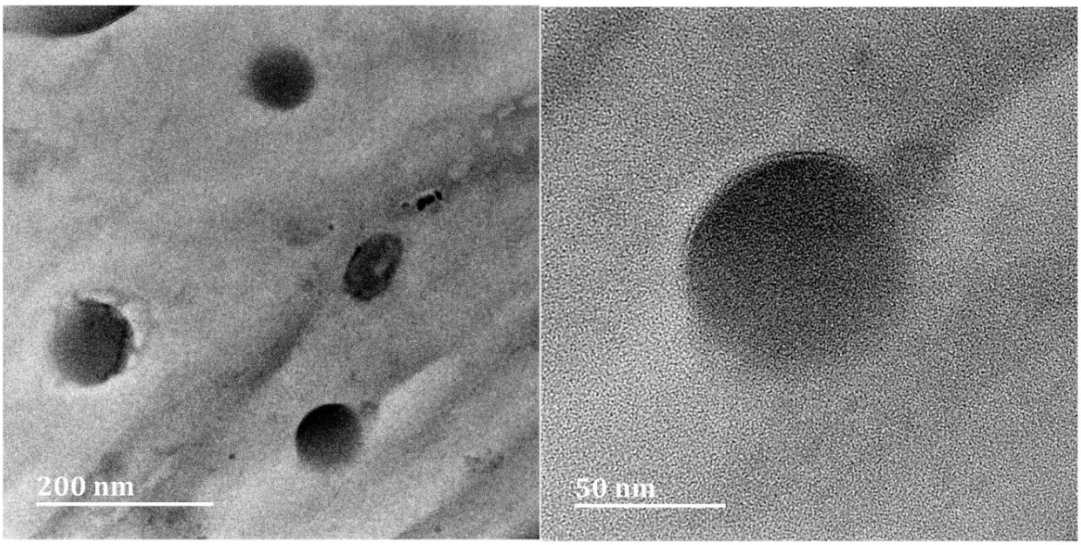

Figure 4 Morphology of amphiphilic CT nanoparticles

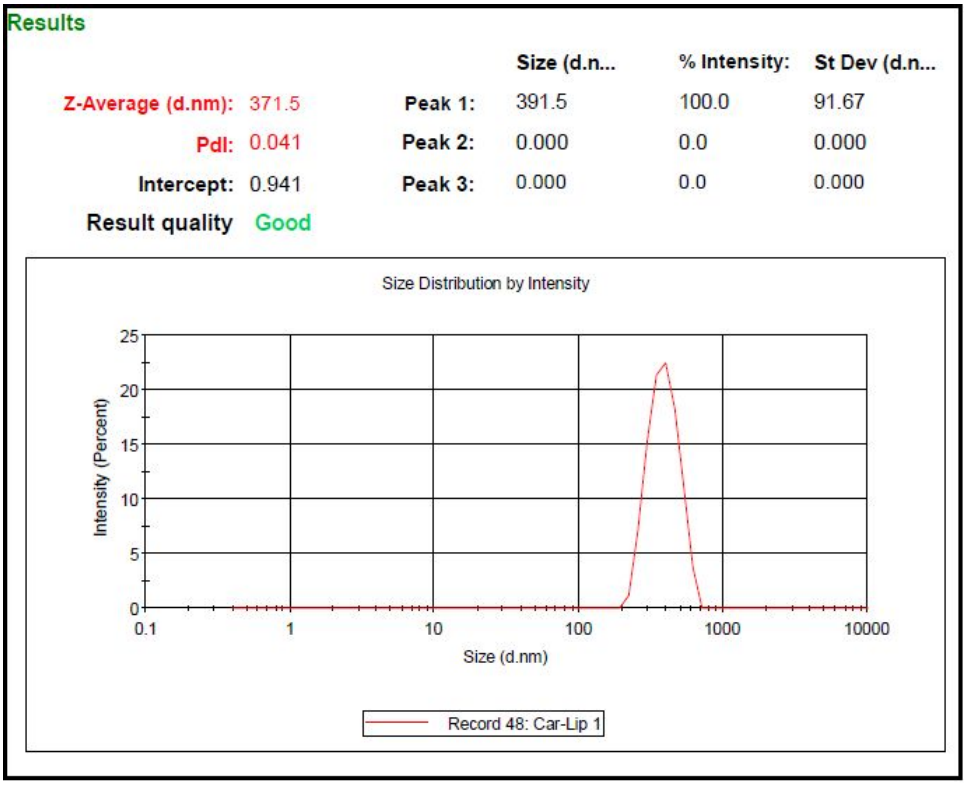

Figure 5 DLS profile: size distribution of CT nanoparticles with PDI:0.041

The characteristic amphiphilicity of the CT provides an chance for itself to self-assemble into organic nanoparticles in water. The TEM study determine the size and morphology of the self assembled nanoparticles (Scale bars: 200 nm and 50 nm) (Fig. 4). The TEM image shows that the CT nanoparticles aggregates into approximate spherical particles in aqueous solution, and the size determined by TEM is about 70 ± 8.0 nm, The DLS results in (Fig. 5) show that the CT nanoparticles solution forms aggregates and the mean hydrodynamic diameter of CT nanoparticles aggregates is about 371.5 nm with a narrow unimodal size distribution. This size is smaller than that measured by DLS due to the shrinkage of CT nanoparticles in a drying non-solvated state during TEM sample preparation. The solution of CT nanoparticles was stored at 4°C in refrigerator. The value of PDI is always under 0.041 at room temperature (Fig. 5) . The results demonstrate that CT nanoparticles are extremely stable during storage.

The CTAuNPs was formed by the addition of an aqueous solution of CT to chloroauric acid solution. After stirring the solution at room temperature, $NaBH_4$ was added dropwise. Fig. 6 shows the synthesis of CTAuNPs.

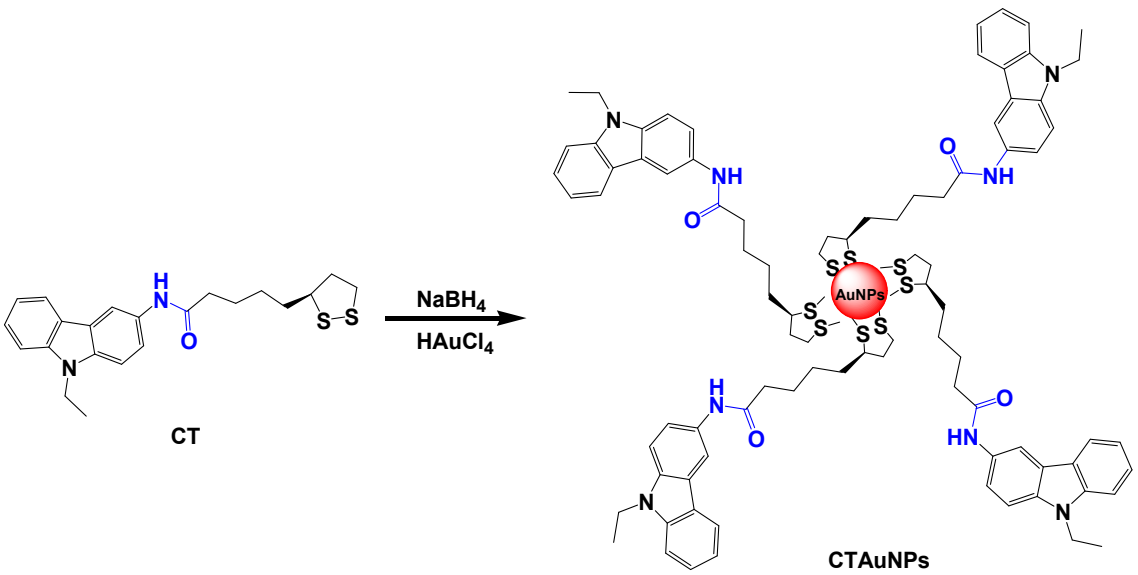

Figure 6 The outline for the synthesis of CT capped gold nanoparticles (CTAuNPs)

The formation of gold nanoparticles was initially confirmed when the solution turned into ruby red color. In Fig. 7 the UV–vis spectra of CTAuNPs is shown. The characteristic peak at 530 nm (Fig. 7curve a) indicates the formation of gold nanoparticles which was due to thesurface plasmon excitation of gold nanoparticles[26]. A bathochromic shift with the

appearance of a broad peak at 552 nm (Fig. 7 curve b) was observed due to the aggregation and surface modification of gold nanoparticles. When carbazole interacted with the gold nanoparticle, the ruby red color rapidly changed into blue.

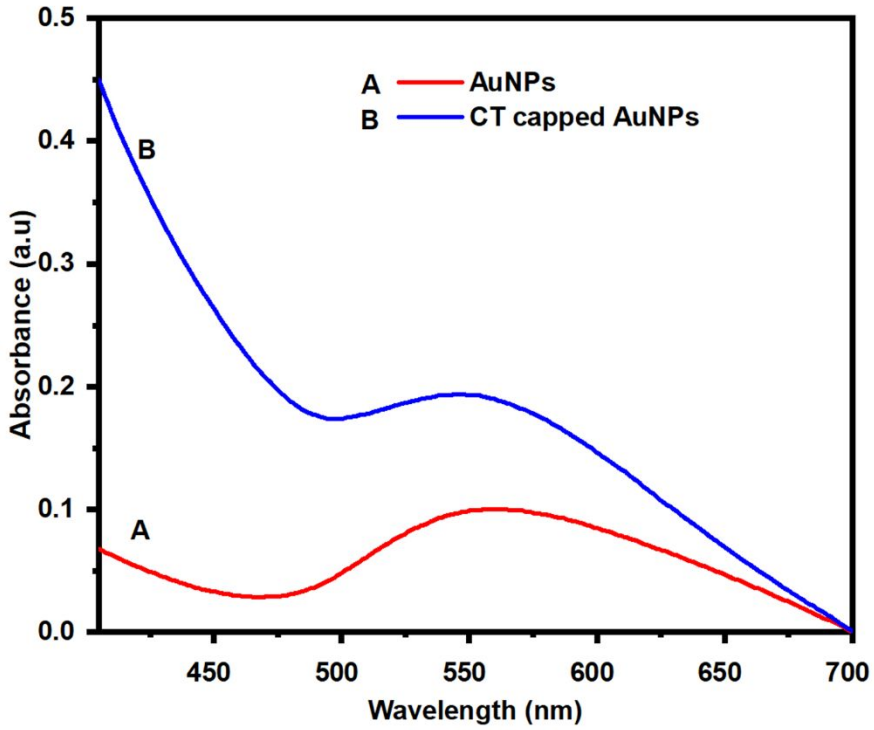

Figure 7 UV-vis spectra of gold nanoparticles line (A) (red color) and CT capped gold nanoparticles line (B) (blue color)

The UV-vis spectrum of the synthesized gold nanoparticle was determined. The size and shape of the nanoparticle were observed with TEM and supported by hydrodynamic size. Zeta potential measurements were observed using Dynamic Light Scattering (DLS) instrument. The observed nanoparticles were mono-dispersed and exactly spherical or nearly spherical with size ranging from 5-10 nm (Fig. 8). Also, spherical shaped gold nanoparticles were observed.

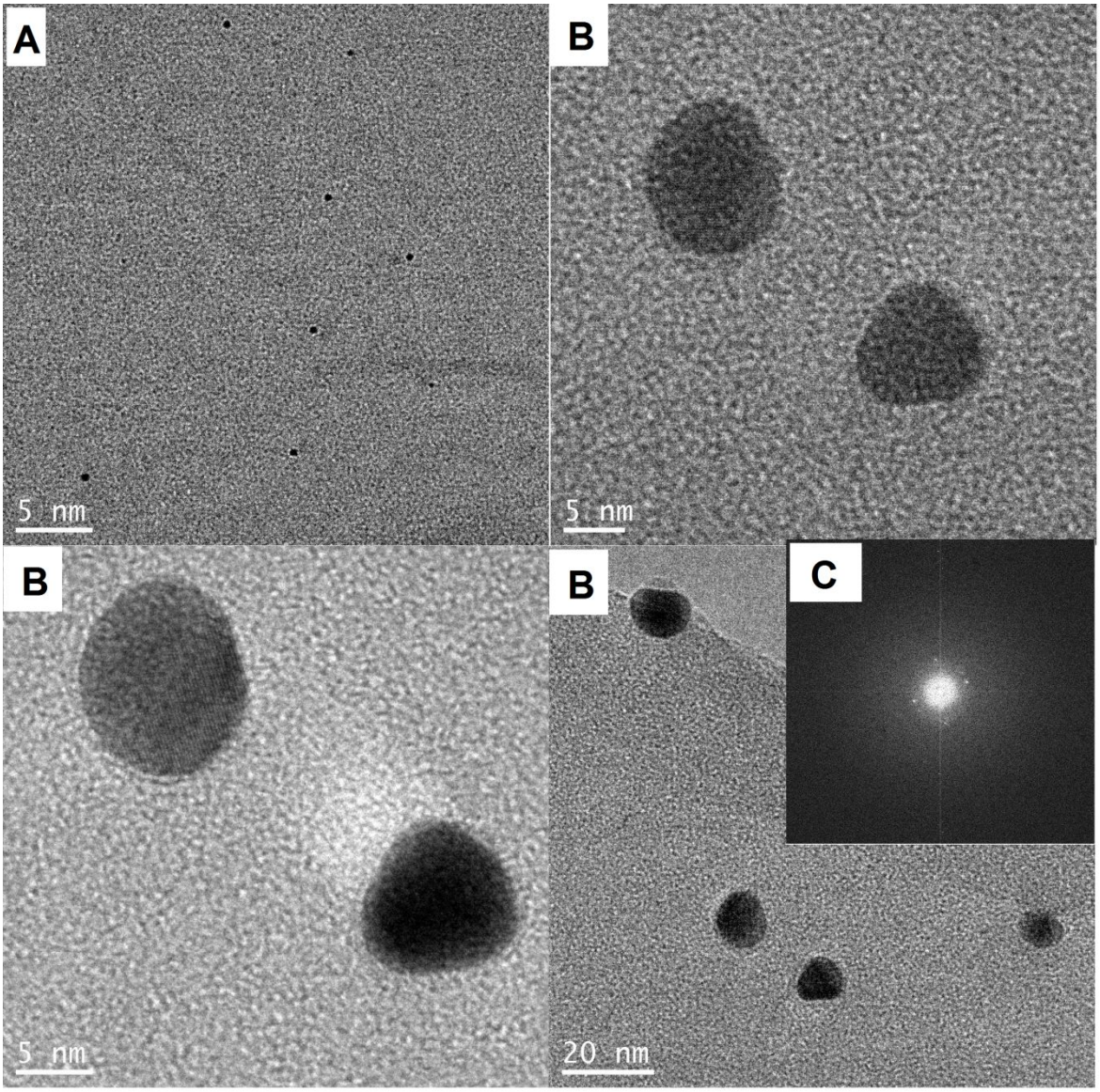

Figure 8 HRTEM images of (A) gold nanoparticles, (B) gold nanoparticles capped with CT, and (C) a part of spherical gold nanoparticle and its corresponding fast Fourier transformed image

Zeta potential is an indication of colloidal stability[27]. Zeta potential of nanoparticles with >+30 mV or < -30 mV is more stable. Colloids having a lower zeta potential results in aggregation due to Van Der Waals forces[27]. HRTEM and DLS adopt different principles for the measurement of particle size. Hence the particle size measured by HRTEM and DLS differs in the margin. Zeta potential was found to be -0.172 mV (Fig. 9B) which shows its least stability. The average hydrodynamic particle size by DLS showed 45 nm (Fig. 9A) which is identical to that observed by HRTEM.

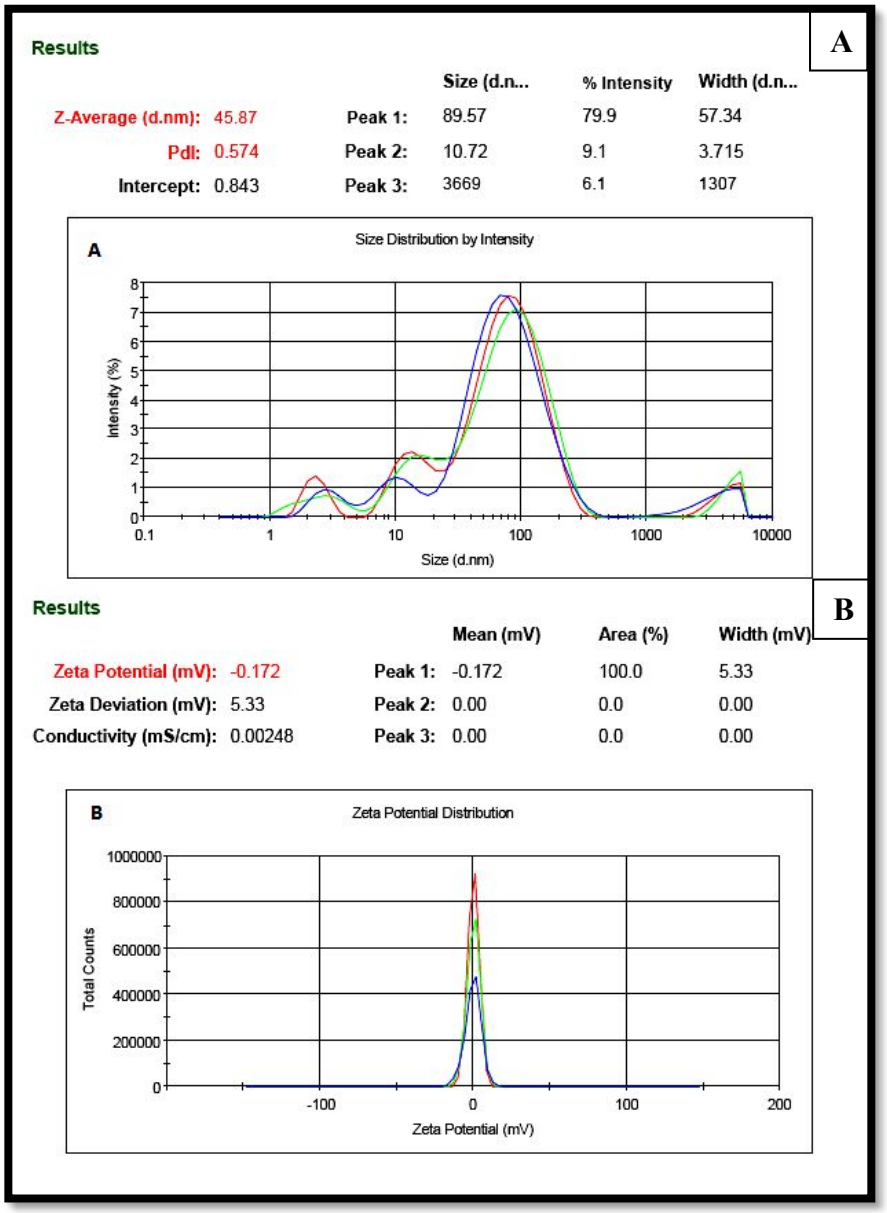

Figure 9 (A) Particle size distribution of CTAuNPs by DLS method **(B)** Zeta potential measurement by Zeta sizer

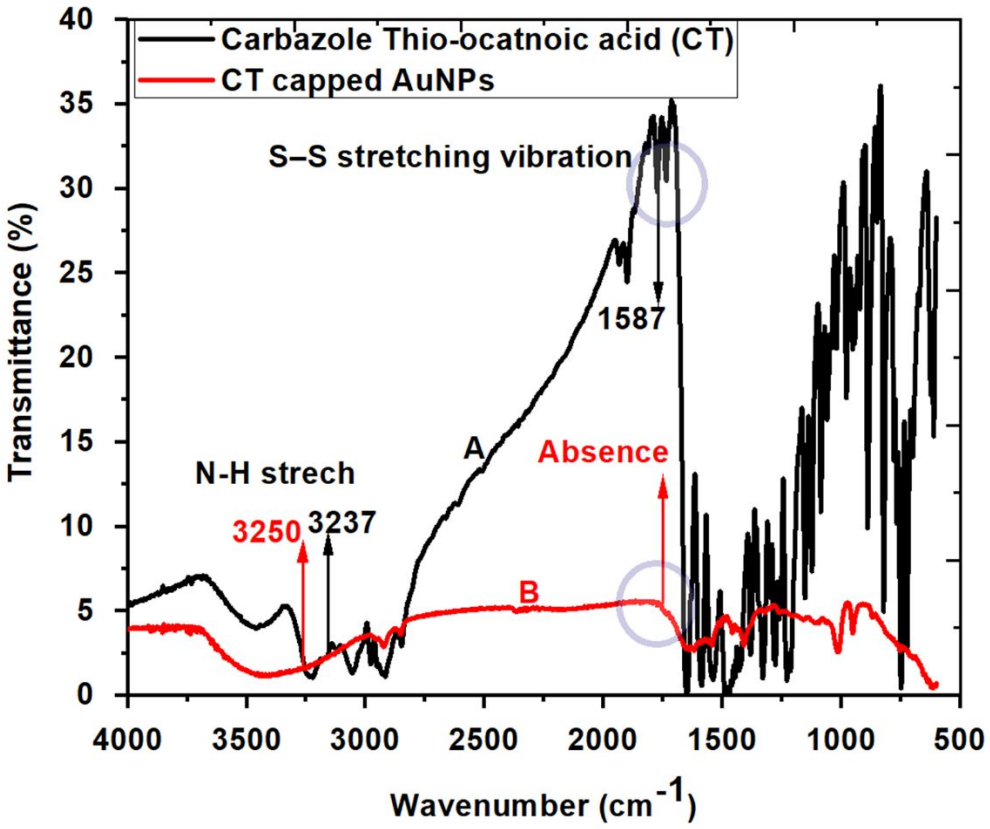

Figure 10 The FTIR Profile of CT (line A) and CTAuNPs (line B)

Fig.10 shows the FTIR spectra which compares the spectra of CT and CTAuNPs. A stretching frequency at 3237 and 1587 cm^{-1} confirmed the NH and S-S functional groups of CTN. The NH band was observed for CTAuNPs, but it was shifted to higher values. Also, the sulfur bond presenting in CT was absent thereby containing an attachment of CT into the gold surface. The S-S group was present in the IR spectra as indicated in Fig 10A and B indicating that it did not participate in any linkage or interaction with the gold surface .

***In vitro* assays**

The anticancerpotential of CTN and CTAuNPs was determined using a liver carcinoma derived (HepG2) cell line. The antiproliferative activities were screened using the MTT assay.

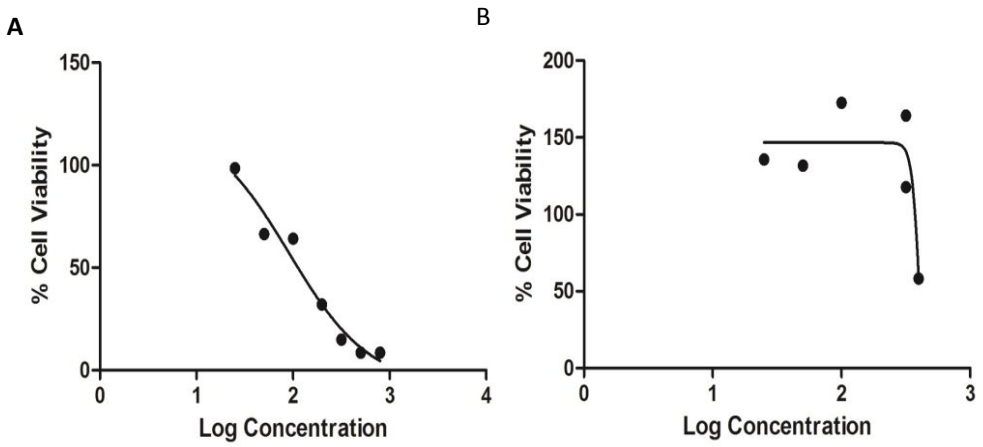

Figure 11 MTT evaluation of cell viability for CTN (A) and CTAuNPs (B) in HepG2 cells

The decrease in cell viability after exposure for 6 hours was dose-dependent with higher concentrations displaying the most significant loss to cell viability. IC_{50} values obtained for CTN and CTAuNPs were 91.3 µg/mL and 432 µg/mL respectively (Fig. 11). While gold-capped nanoparticles easily penetrate cell membranes and are often described as an effective drug carrier, our data indicate that the self-assemble organic CTN displayed greater effectiveness in decreasing cell viability when compared to the gold derivative. Gold nanoparticles display diverse and unique properties that may contribute to cell protective mechanisms after acute treatments such as anti-oxidant defense mechanisms and altered the energy flux. Therefore, only CTN was selected for further biological assessment.

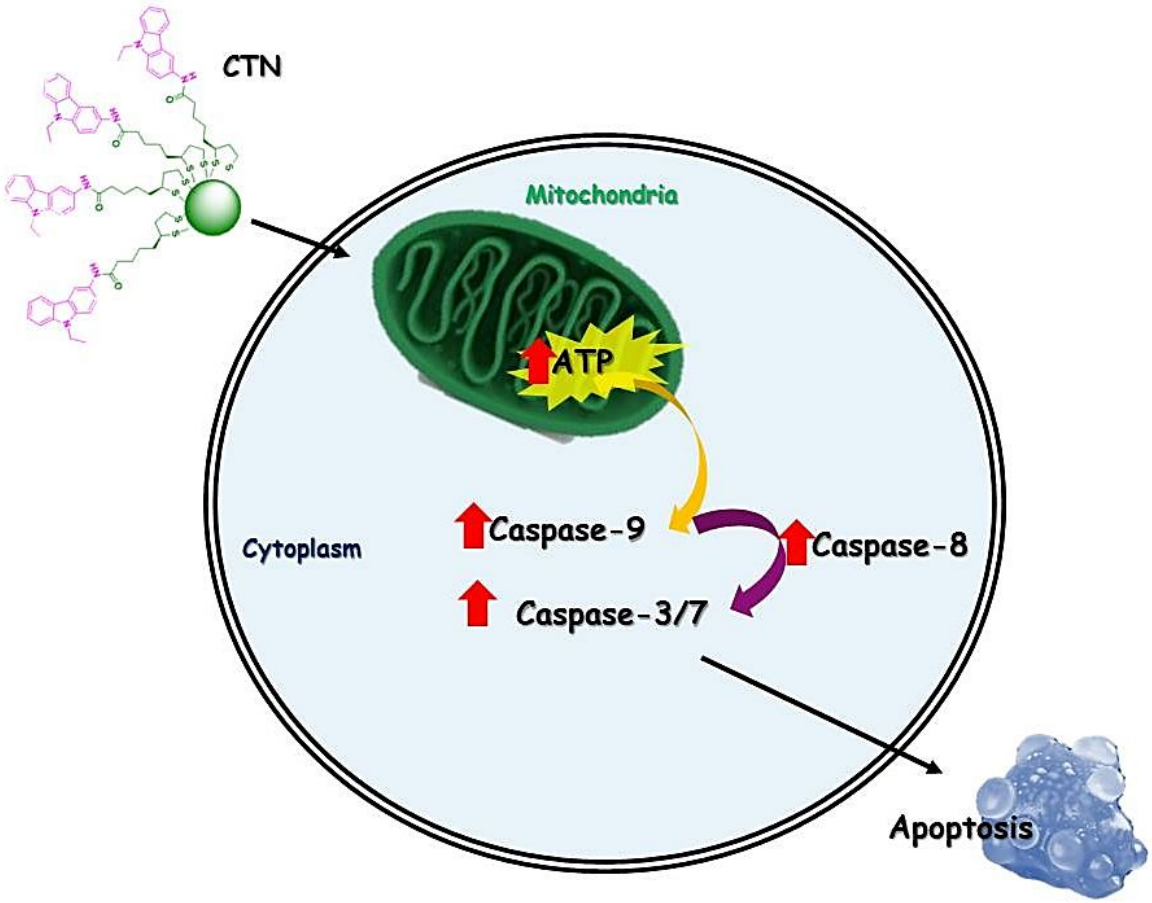

Figure 12 Schematic representation of CTN induced apoptosis

The cytotoxic potential of carbazole derivatives has already been established in several *in vitro* models[28]. Our innovative conjugation of a carbazole to the antioxidant and mitochondrial stimulator i.e., α-lipoic acid has sown a profound effect on caspase initiation and activation (a marker for apoptosis). Apoptosis or programmed cell death regulates the elimination of damaged cells to maintain homeostasis. Caspases are critical facilitators of apoptosis as they initiate and execute the process via two pathways: the extrinsic and the intrinsic pathway. The extrinsic pathway is stimulated by ligands binding to receptors that regulate downstream adaptor molecules resulting in caspase 8 activation (Fig. 12). The intrinsic pathway involves the binding of caspase 9 to the apoptotic protease-activating factor-1 (APAF-1) apoptosome complex in response to mitochondrial signals such as membrane depolarization. Both pathways result in the activation of executioner caspases, caspase 3/7.

Our data indicates the enhanced activity of executioner caspases 3/7 (Fig. 13C). The initiators of the extrinsic (Fig. 13A) and intrinsic (Fig. 13B) apoptotic pathways are also up-

regulated. It is intriguing that caspase activity increases in a dose-dependent manner but drastically decreases at the highest CTN concentration. We speculate that this may be due to membrane receptor saturation and rapid ATP depletion (Fig. 14).

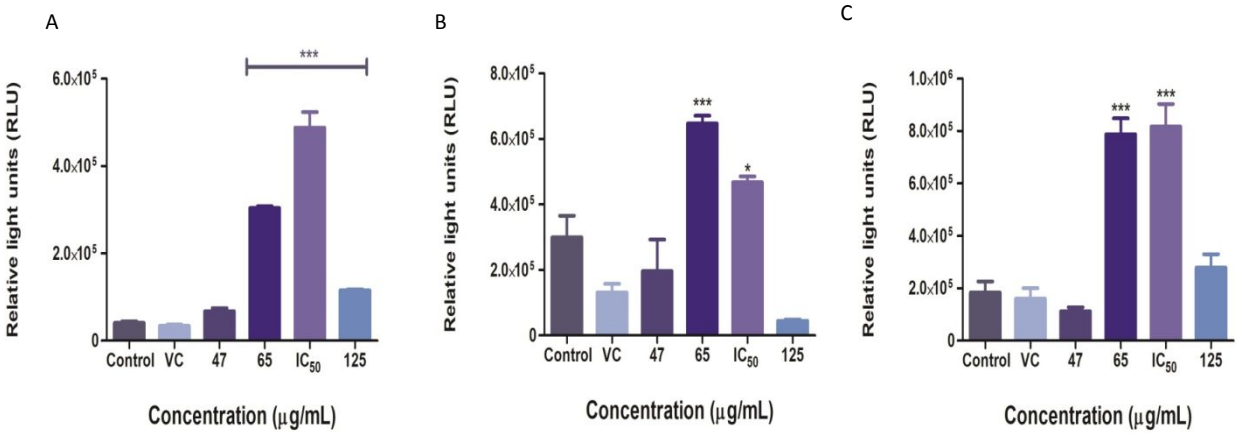

Figure 13 (A) CTN increased the activity of the extrinsic caspase 8,**(B)** intrinsic caspase 9 and **(C)** executioner caspases 3/7. Key: *** p<0.001 p<0.05

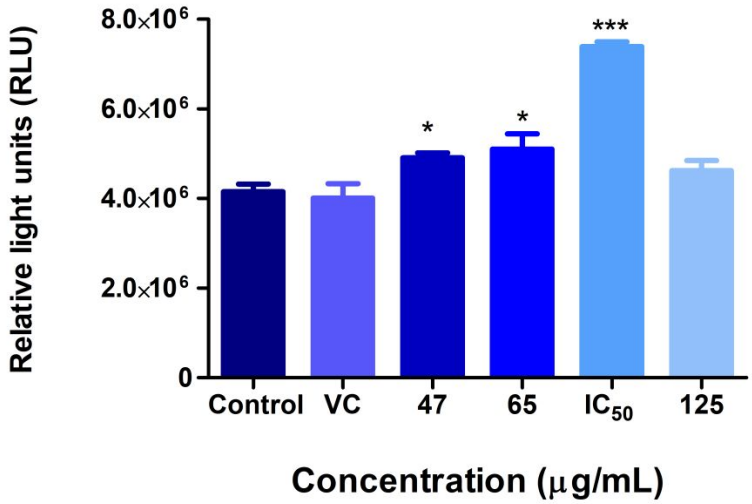

Figure 14 Effect of CTN on ATP detection

The plasma membrane integrity was evaluated by determining LDH release into the supernatant. Plasma membrane leakage is strongly correlated with overt cytotoxicity and

necrotic cell death. We observed no significant changes to the levels of released LDH (Fig. 15) suggesting that apoptosis was responsible for cell death and not necrosis. The results are in agreement with the caspase activity assays. Triggering apoptosis without overt necrosis would be the preferred means of destroying cancer cells as it dampens many of the damaging side effects. This is important to normal healthy cells that may not be affected by the drug and hence eliminate any unwanted side effects generally associated with chemotherapy.

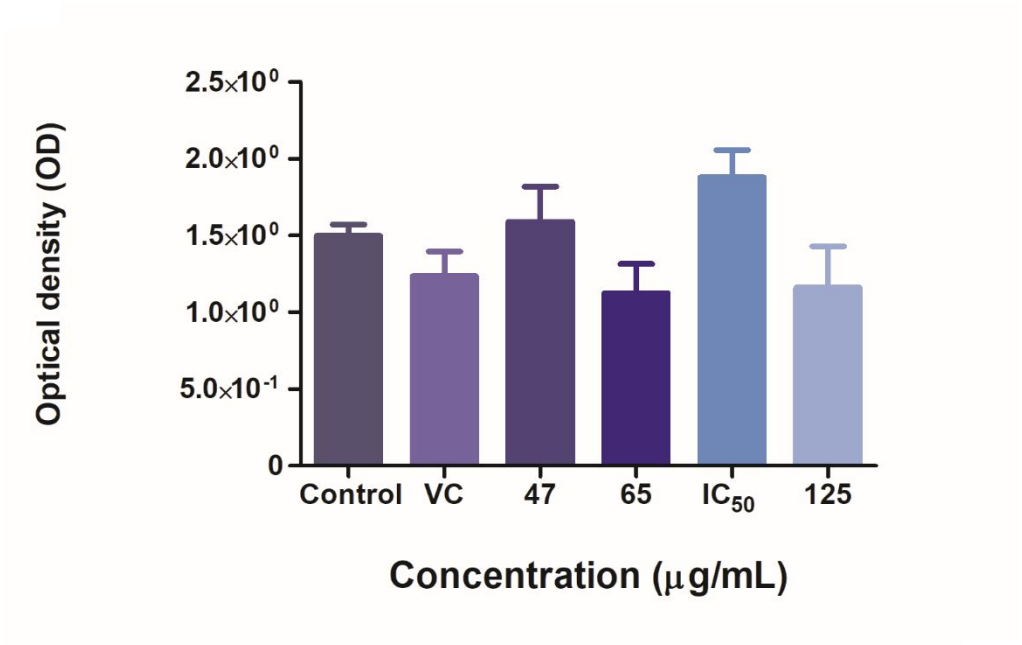

Figure 15 Effect of CTN on LDH leakage

In silico analysis to investigate the other anticancer target

Molecular docking and molecular dynamics are the *in-silico* approaches to predict the ligand binding pose inside the target protein or host molecule[29]. The application of molecular docking to predict the therapeutic and metabolic profiles has been well documented[30]. In the present study, molecular docking and molecular dynamics have been employed to investigate the therapeutic anticancer potential of carbazole, lipoic acid, and carbazole-thiooctanoic acid.

Molecular docking has been used as a tool to evaluate the interaction and geometric conformation of a ligand-biological target[31]. The potential mechanism of carbazole is the inhibition of epidermal growth factor receptor (EGFR). EGFR is a validated target for the treatment of cancer[28, 32]. Therefore, carbazole, lipoic acid, and carbazole-thiooctanoic acid were docked into the binding site of EGFR to explore the anticancer therapeutic potential.

Carbazole, lipoic acid, and carbazole-thiooctanoic acid were respectively shown the docking scores of -7.2, -4.8, and -7.9 kcal/mol **(Table 1).** The range of root mean square deviation for each of the molecule [aminocarbazole (AC), lipoic acid (LA), and carbazole-thiooctanoic acid (CT)] from the top-ten ranked pose is shown in Table 1. Carbazole-thiooctanoic acid has shown the highest docking scores of (-7.9 kcal/mol) in comparison to carbazole and lipoic acid. Carbazole-thiooctanoic acid (CT) is the combined molecular fragments of carbazole and lipoic acid. The combined molecular feature may be responsible for the achievement of the highest molecular docking score. The interacting residues of EGFR and its interaction with mono CT were shown in Fig 16 and Fig 17. Val21, Leu22, Ala47, Thr92, Asp157, and Arg143 were found to be binding site residues for carbazole-thiooctanoic acid at the binding site of EGFR in molecular docking.

Table 1. Molecular docking scores of the molecules (Aminocarbazole, Lipoic acid, and CT)

No.	Molecule	Docking scores	RMSD (lb)	RMSD (ub)
1.	Aminocarbazole	-7.2	0.00 – 1.598	0.0 – 4.567
2.	Lipoic acid	-4.8	0.00 – 4.479	0.0 – 5.888
3.	CT	-7.9	0.0 – 3.202	0.0 - 6.032

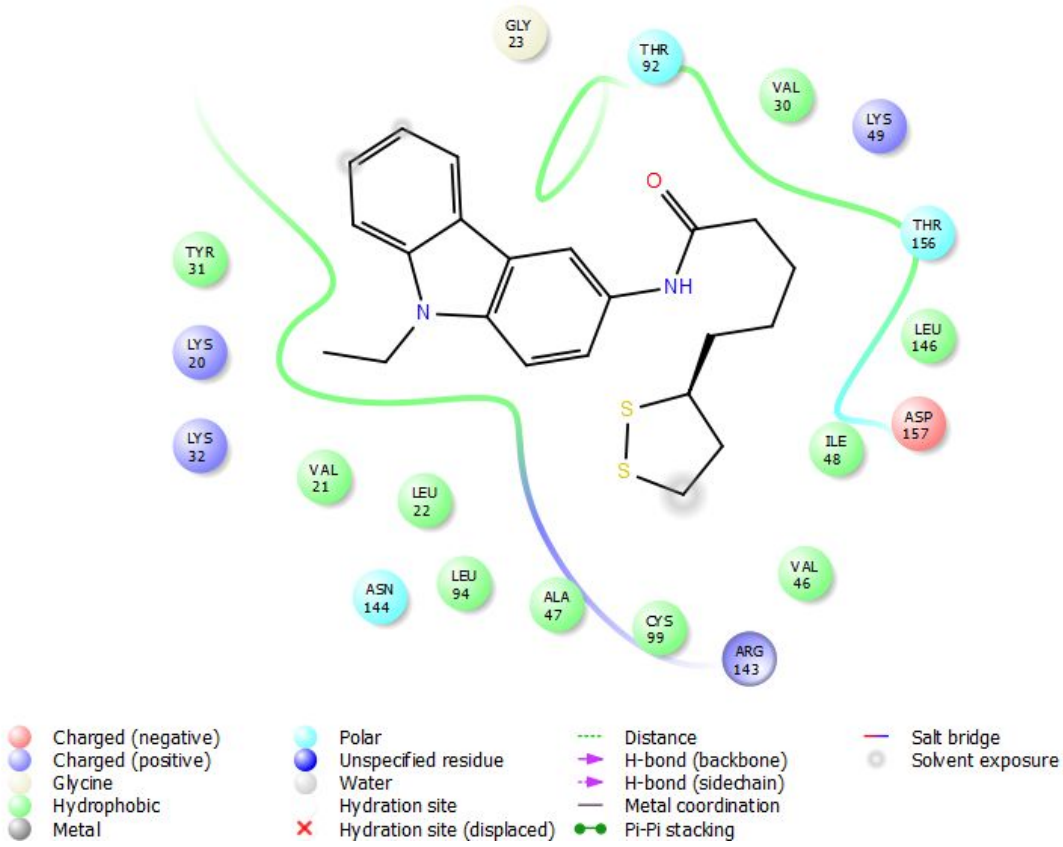

Figure 16. The interaction pattern of CT with EGFR in molecular docking

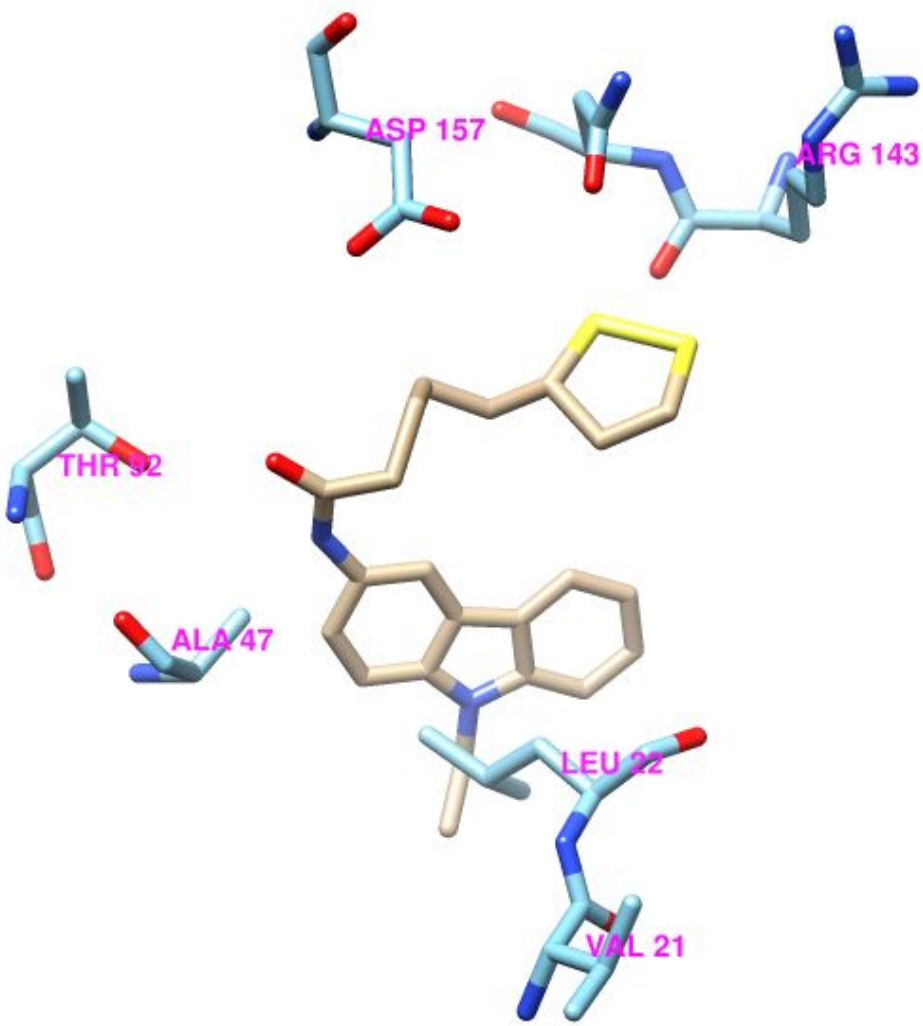

Figure 17. The binding landscape of CT inside the ligand binding site of EGFR in molecular docking

The highest docking score of -7.9 kcal/mol has been obtained for the complex of carbazole-thiooctanoic acid with EGFR in molecular docking. Therefore, the complex has been subjected to molecular dynamics simulation. The results of molecular dynamics simulation help to ensure the binding affinity of the ligand and stability of the complex from the estimated of energy components. Molecular dynamics simulation was carried out for the complex of carbazole-thiooctanoic acid with EGFR in AMBER 18[33]. Initially, the molecular docking complex was pre-treated in Chimera before submitting to molecular dynamics[34]. The ligand-bound complex was used as an initial geometry for molecular dynamics. The ligand and the protein were parametrized in Antechamber and *tleap*[35]. The complex was neutralized by adding (Na^+/Cl^-) as counter ions and the complex was solvated using TIP3P water model[36]. The minimization of the complex was carried out for 200 steps. The heating

and equilibrium were conducted at 300K. Then, the simulation of the complex system was carried out for 5 ns[37]. The results of the trajectories were saved for every 1ps and were analyzed using CPPTRAJ module[38]. After the 5 ns simulation, the binding free energy of the ligand-protein complex (carbazole-thiooctanoic acid with EGFR) was estimated by the Molecular Mechanics/Poisson Boltzmann Surface Area (MM/PBSA) method. The estimated energy components were depicted in Table 2. The estimated VDWAALS components were found to be (-45.31 kcal/mol). The stability and flexibility of the complex were analyzed from the RMSD and RMSF plot (Fig 18). Moreover, the complex has shown a strong binding free energy of (-39.86 kcal/mol) from the binding free energy calculation **(Table 2)**. This strong binding affinity of carbazole-thiooctanoic acid with EGFR shows its therapeutic potential as an anticancer agent.

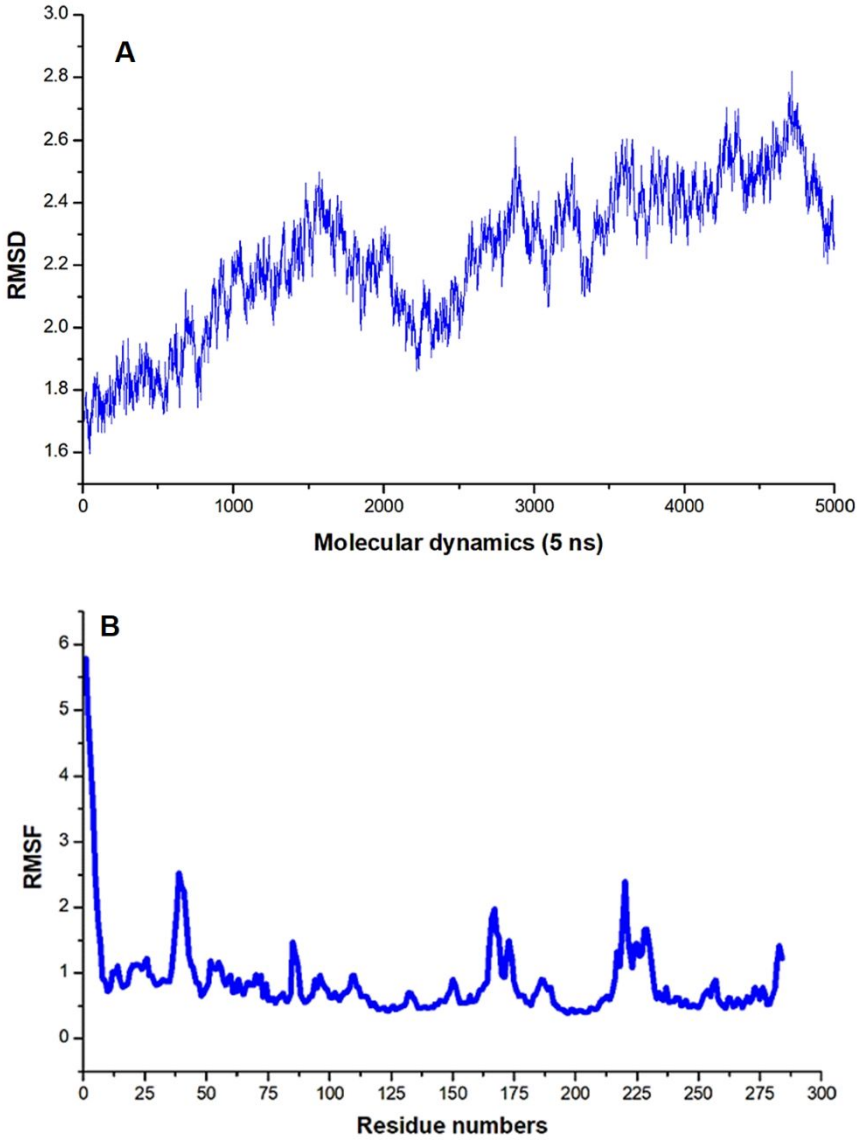

Figure 18. (A) RMSD and **(B)** RMSF plots of the carbazole-thiooctanoic acid (CT) with EGFR complex in molecular dynamics simulation

Table 2. The energy components of CT-EGFR complex in molecular dynamics simulation

Energy Component	Average	Std. Dev.	Std. Err. Of Mean
VDWAALS	-45.3100	3.8646	0.3865
EEL	-15.7461	7.0271	0.7027
EGB	27.0712	4.9542	0.4954
ESURF	-5.8744	0.3937	0.0394
DELTA G gas	-61.0561	9.8450	0.9845
DELTA G solv	21.1968	4.6821	0.4682
DELTA TOTAL	-39.8593	6.1557	0.6156

6. Conclusion

In this study, Utilizes self-assembly amphiphilic carbazole-thiooctanoic acid (CTN) nanoparticles i.e., aminocarbazole (mutagen) and lipoic acid (antioxidant) as two in one molecule to investigate the biochemical mechanism of the binary molecule on human cancerous liver (HepG2) cells. The carbazole-thiooctanoic acid capped gold nanoparticles (CTAuNPs) were synthesized, characterized, and apoptotic induction activity of the same was studied. To prove the interaction between disulfide and AuNPs, the spectroscopic analysis was performed. It showed the disulfide group of carbazole lipoic acid acting as a potential site to conjugate with the gold surface at nanoscale, resulting in carbazole capped gold nanoparticles. The CTN increased the activity of the extrinsic caspase 8, intrinsic caspase 9 and executioner caspases and LDH release was not altered significantly suggesting apoptosis instead of necrosis in liver carcinoma (HepG2) cells. The results indicated that self-assembled carbazole nanoparticles CTN induces apoptosis in the absence of overt necrosis in liver carcinoma (HepG2) cells and it may be a novel anti-cancer agent. Moreover, the *in-silico* studies like molecular docking and molecular dynamics have shown the strong binding affinity for carbazole-thiooctanoic acid (CT) with EGFR. In post-dynamics, this complex has shown substantial stability during the simulation. Therefore, carbazole-thiooctanoic acid may act as potential anticancer agents.

2. Materials andMethods

2.1. Chemicals and reagents

Gold (III) chloride trihydrate ($HAuCl_4.3H_2O$), 9-ethyl-3-amino carbazole, Hexafluorophosphate Benzotriazole Tetramethyl Uronium (HBTU), Diisopropylethylamine (DIEA), lipoic acid, and $NaBH_4$ were procured from Sigma Aldrich, South Africa. Other chemicals were procured as analytical grade and do not require purification. Reagents used for the study were prepared using distilled water. Glasswares were washed thoroughly using aqua regia followed by double distilled water.

2.2. Synthesis of novel carbazole thiooctanoic acid (CT)

15 ml of Dimethylformamide (DMF) and 5ml of Tetrahydrofuran (THF) was used to solubilize lipoic acid (0.55 g, 2.75 mmol) and then added with HBTU (1 g, 3.05 mmol), DIEA (1 ml, 6.00 mmol) and 9-ethyl-3-amino carbazole (0.56 g, 2.7 mmol). The resultant mixture was fully dissolvedusing magnetic stirrer at room temperature. TLC analysis was performed to check for conjugation. 50 ml of distilled water was added to the resultant mixture and then extracted with ethyl acetate (25 ml) for three times. Ethyl acetate layer was combined and then dried by passing it through anhydrous sodium sulfate followed by evaporation to yield the crude product. Finaly, a white solid CT was obtained after purification using column chromatography (50:50 EtOAc/Hexane). Yield: 1.10g (92%); mp: 120 °C; IR (KBr, cm^{-1}): 3462.01, 3237.92, 3058.40, 2917.84, 2513.46, 2513.46, 1900.406, 1773.85, 1736.05, 1650.38, 1587.43, 1542.65, 1485.11, 1382.07, 1277.01, 1228.44, 1152.46, 1123.774, 1085.725, 1060.128, 1020.12, 1020.128, 978.56, 888.97, 821.95; ^{1}H-NMR (400 MHz, $CDCl_3$): δ (ppm) 1.35 (m, 2H), 1.39 (s, 3H), 1.56 (q, 2H), 1.68 (m, 2H), 1.80 (m, 2H), 2.40 (t, 2H), 2.62 (m, 1H), 3.34 (m, 2H), 3.5 (t, 1H), 4.35(q, 2H), 7.0-7.1 (s, 1H), 7.16-7.19 (t, H), 7.29 (s, 1H), 7.31.(s, 1H), 7.37-7.36 (d, 1H), 7.418-7.41 (m, 1H), 8.20 (d, 1H), 8.42 (t, 1H); ^{13}C-NMR (400 MHz, $CDCl_3$,): δ (ppm) 171.00, 140.44, 137.23, 129.61, 125.85, 123.02, 122.75, 120.66, 119.49, 118.73, 112.91, 108.53, 108.45, 58.43, 40.28, 48.48, 37.39, 37.37, 34.69, 33.94, 28.93, 25.43, 24.94, 13.80.

2.3. Formation of carbazole nanoparticles (CTN)

At room temperature, novel carbazole thio octanoic acid (CT) twin bioactive molecules (25 mg) was dissolved in acetone (20 mL). All the prepared CT solutions were syringe filtered

(pore size 0.22 µm). Subsequently, the antisolvent deionized water (20 ml) was added in drops to the solution and stirred gently for half an hour, and the nanoparticle was precipitated. This technique was termed as antisolvent precipitation technique. The appearance of turbidity indicated the formation of amphiphile CT Nanoparticles (CTN) from CT twin bioactive molecules.

2.4. Characterization of carbazole nanoparticles (CTN)

Particle size (z-average diameter, d/nm), polydispersity index (PDI) Fig. 5, and zeta potential of the precipitated nanoparticles were analyzed using dynamic light scattering (DLS) (Zetasizer Nano ZS, Malvern Instrument Ltd., UK) at 25˚C. Particle size and shape of the nanoparticle were characterized by transmission electron microscopy (TEM) Fig. 4. CTNNPs (1µl) were kept on formvar coated grids, air-dried, and observed at 100 kV for TEM (JEOL 1010 TEM using a Megaview III camera and iTEM software) studies.

2.5. Synthesis of novel carbazole thiooctanoic acid capped gold nanoparticles (CTAu NPs)

The sodium borohydride reduction method was adopted to synthesize gold nanoparticles[14]. Briefly, 0.01 g of $NaBH_4$ was employed to reduce tetrachloroauric acid (10^{-4} M) leading to the synthesis of gold nanoparticles of 5nm in diameter. The resultant nanoparticle solution was ruby-red in colour. Subsequently, 10^{-3} M aqueous solution of CT was used as a capping agent for gold nanoparticles.Then the solution wasrepeatedly centrifuged (10,000 rpm for 1hour) to purify the carbazole thiooctanoic acid capped gold nanoparticles.

The absorption spectra (200nm - 800nm)of the capped gold nanoparticles solution was measured using a UV-vis spectrometer (Varian Cary-50 UV spectrophotometer linked to a TCC-240A Shimadzu heating vessel temperature controlled cell holder).To analyze the size and shape, 1 µl of the CTAu NPs was kept on formvar coated grids, air-dried, and observed using TEM. For FTIR studies, CTAu NP was purified by centrifugation (10,000 rpm for 10min) and the resultant pellet was washed thrice using distilled water (20 ml). Then the FTIR spectra were recorded using Varian 800 FTIR spectrophotometer.Particle size and zeta potential were evaluated using a Differential Light Scattering Malvern Zetasizer Nano ZS (Malvern Instruments Ltd, UK) Merck 2423 instrument.

2.6. Cell culture

The HepG2 human liver carcinoma cells were grown in 25cm^3 culture flasks (37°C, 5% CO_2) in complete culture media (CCM, Eagles Minimum Essential media, supplemented with 10% fetal calf serum, 1% L-glutamine, and 1% penicillin-streptomycin-fungizone) until to obtain 90% confluent. Then, the cells were harvested by trypsinization and used for the relevant assays.

2.7. Cell viability

MTT assay was adopted to analyze the cell viability. HepG2 cells (15,000 cells/well) were seeded in a 96 well microtitre plate and incubatedovernight to adhere to the plate. The cells were incubated for 6 hrs with varying concentrations of CTN and CTAu (0-750 µg/mL) in five replicates. The plate wasincubated at 37°C for 4 hours after the addition of 120 µl of MTT/CCM solution (5mg/mL) into each well. Supernatants were decanted, added with 100µl of DMSO,and incubated for 1 hr (37°C). The absorbance was read using a spectrophotometer (Bio-Tek µQuant) at a wavelength of 570/690 nm. The percentage of viable cells was measured and a dose-response curve was generated from which the IC_{50} value was extrapolated.

For further analysis, the cells were exposed to sub and overt IC_{50} concentrations for a dose-dependent study of the novel compound. All these experiments were performed thrice independently in triplicate.

2.8. ATP assay

HepG2 cells (20,000cells) were seeded into each well of the 96 well-plate along with 20µl CellTire Glo™ reagent (Promega, Madison, USA) and incubated in dark for 30 mins at room temperature (RT). The luminescent signal was then read using a Modulus™ microplate luminometer (Turner Biosystems, Sunnyvale, USA). The strength of the signal corresponds to the concentration of intracellular ATP. Results werementioned in mean relative light units (RLU). All these experiments were repeated thrice in triplicate.

2.9. Caspase assay

The Caspase Glo® 8, 9 and 3/7 Assay kits (Promega, Madison, USA) were used to detect caspase activity. The same procedure was followed for the listed caspases: treated and untreated cells (20,000 cells) were seeded into each well of the 96 well-plate along with20µl

of Caspase Glo® reagent(prepared as per the instruction manual) and incubated in dark for 30 mins at RT. Theluminescence was detected and quantified using a Modulus™ microplate luminometer (Turner Biosystems, Sunnyvale, USA). The data wererepresented as mean relative light units (RLU).

2.10. LDH assay

The LDH cytotoxicity detection kit (Roche, Mannheim, Germany) was employed to determine cell death that occurred through membrane damage. Briefly, the supernatant (100µl) of control and treated cells were added to the wells of 96-well microtitre plate followed by substrate mixture and left for 25 mins at RT, for the reaction to occur. Here substrate mixture has a catalyst (diaphorase/NAD+) and dye (INT/sodium lactate). Optical density was recorded spectrophotometrically at 500nm (Bio-Tek uQuant). The results are expressed in mean ± standard deviation (SD) of optical density. All these experiments were repeated thrice in triplicate.

3. Molecular docking

Molecular docking is used as a tool to view the interaction/selectivity of a ligandto the active site pocket of protein[15]. The 3D structure of EGFR (PDB code:**6JXT**) was acquired from the Protein Data Bank[16]. Thestructure of carbazole, lipoic acid, and CT was built using ChemDraw software. To optimize the geometry of ligand, MM2 force field was employed17. The docking was carried out to study the interactions and the binding affinity of barbazole, lipoic acid, and CTwith EGFR. A grid box with the spacing of 1 Å and size of 15 × 15 × 15 pointing in x, y, and z directions was defined at the proximity of bound ligand in EGFR using the standard protocol[18,19]. Then the molecules were docked using AutoDockVina[17] with standard docking parameters. The Lamarckian Genetic Algorithm was used as the search algorithm with standard parameter values. The ideal docked conformation was chosen for further investigations. Details of docking parameters are described in our previous communications[21,22] PyMol[23], Discovery Studio Visualizer[24], and LigPlot+ [25] were employed to visualize and analyse the structure of the docked complex.

4. Statistical analysis

Biological experiments were conducted thrice (independently) in triplicate. Statistical data was evaluatedby one way ANOVA and the Bonferroni test for multiple group comparisons.

Results are expressedin mean ± standard deviation (SD) unless mentioned. Results with $p<0.05$ are statistically significant.

6. Acknowledgments

Authors gratefully acknowledges the University of KwaZuluNatal and University of the Free State, South Africa (SA) for the financial support and infrastructural facilities for this project. K.A. is grateful to National Research Foundation (NRF), SA for the research funding in the form of NRF/DSI Innovation Post-Doctoral Research Fellowship (grant no. 120677). All computational tasks were carried out using the software resources of the Centre for High Performance Computing, Cape Town, South Africa.We are grateful to the Electron Microscope Unit, UKZN for TEM measurements, and T. Govender (Department of Pharmacology, UKZN) for DLS studies.

Competing Interests:

The authors declare no competing interests.

References

(1) Hao, G.; Sun, J.; Wei, C. Studies on interactions of carbazole derivatives with DNA, cell image, and cytotoxicity. *Bioorganic & Medicinal Chemistry.* **2018***,* 26, 285-294.

(2) Yuan, Y.; Cai, T.; Xia, X.; Zhang, R.; Chiba, P.; Cai, Y. Nanoparticle delivery of anticancer drugs overcomes multidrug resistance in breast cancer. *Drug Delivery***. 2016**, 23, 3350-3357.

(3) Zhang, T.; Huang, P.; Shi, L.; Su, Y.; Zhou, L.; Zhu, X.; Yan, D. Self-Assembled Nanoparticles of Amphiphilic Twin Drug from Floxuridine and Bendamustine for Cancer Therapy. *Molecular Pharmaceutics.***2015**, 12, 2328-2336.

(4) Jazayeri, M. H.; Amani, H.; Pourfatollah, A. A.; Pazoki-Toroudi, H.; edighimoghaddam, B. Various methods of gold nanoparticles (GNPs) conjugation to antibodies. *Sensing and Bio-Sensing Research.* **2016**, 9, 17-22.

(5) Namiki, Y.; Takahashi, T.; Ohno, T. Gene transduction for disseminated intraperitoneal tumor using cationic liposomes containing non-histone chromatin proteins: cationic liposomal gene therapy of carcinomatosa. *Gene therapy.* **1998,** 5, 240-246.

(6) Ding, Y.; Zhang, X.; Liu, X.; Guo, R. Adsorption Characteristics of Thionine on Gold Nanoparticles. *Langmuir.* **2006,** 22, 2292-2298.

(7) Manna, A.; Chen, P. L.; Akiyama, H.; Wei, T. X., Tamada, K.; Knoll, W.; Optimized Photoisomerization on Gold Nanoparticles Capped by Unsymmetrical Azobenzene Disulfides. *Chemistry of Materials.* **2003,** 15, 20-28.

(8) Bistri, O.; Reinaud, O. Supramolecular control of transition metal complexes in water by a hydrophobic cavity: a bio-inspired strategy. *Organic & Biomolecular Chemistry.* **2015,** 13, 2849-2865.

(9) Bustamante, J; Lodge, J K; Marcocci, L ; Tritschler, H J; Packer, L; Rihn, B H. α -Lipoic Acid in Liver Metabolism and Disease. *Free Radical Biology and Medicine*, **1998**, 24, 1023-1039.

(10) Qingye, M; Hao. H; Liping, Z; Yixin, Z; Bing, Y; Youqing, S; and Hailin C. Logical design and application of prodrug platforms. *Polym. Chem.* **2019,** 10, 30-6-324.

(11) P. Huang, D. Wang, Y.Su, W. Huang, Y. Zhou, D. Cui, X. Zhu, D. Yan, Combination of Small Molecule Prodrug and Nanodrug Delivery:Amphiphilic Drug−Drug Conjugate for Cancer Therapy, J. Am. Chem. Soc. 2014, 136, 11748−11756

(12) T. Zhang, P. Huang, L. Shi, Y. Su, L. Zhou, X. Zhu, D. Yan, Self-Assembled Nanoparticles of Amphiphilic Twin Drug from Floxuridine and Bendamustine for Cancer Therapy, Mol. Pharmaceutics 2015, 12, 2328−2336

(13) Taylor, R. D.; MacCoss, M.; Lawson, A. D. G. Rings in Drugs. *Journal of Medicinal Chemistry.* **2014,** 57, 5845-5859.

(14) Suchomel, P.; Kvitek, L.; Prucek, R.; Panacek, A.; Halder, A.; Vajda, S.; Zboril, R. Simple size-controlled synthesis of Au nanoparticles and their size-dependent catalytic activity. *Scientific Reports*. **2018**, 8, 4589.

(15) Khan, F. I.; Wei, D. Q.; Gu, K. R.; Hassan, M. I.; Tabrez, S.; Current updates on computer aided protein modeling and designing. *International Journal of Biological MacromoleculeS.* **2016**, 85, 48-62.

(16) Xiao, E. Y.; Ayaz, P.; Zhu, S. J.; Zhao, P.; Liang, L.; Zhang, C. H.; Wu, Y. C.; Li, J. L.; Choi, H. G.; Huang, X.; Shan, Y.; Shaw, D. E.; Yun, C. H.; Structural Basis of

AZD9291 Selectivity for EGFR T790M. *Journal of Medicinal Chemistry.* **2020***,* 63, 8502-8511.

(17) Hanwell, M. D.; Curtis, D. E.; Lonie, D. C.; Vandermeersch, T.; Zurek, E.; Hutchison. G. R. Avogadro: an advanced semantic chemical editor, visualization, and analysis platform. *Journal of Cheminformatics.* **2012,** 4, 17.

(18) Cosconati, S.; Forli, S.; Perryman, A.; Harris, R.; Goodsell, D.; Olson, A.; Virtual Screening with AutoDock: Theory and Practice. *Expert opinion on drug discovery.* 2010*,* 5, 597-607.

(19) Khan, F. I.; Nizami, B.; Anwer, R.; Gu, K. R.; Bisetty, K.; Hassan, M. I.; Wei, D. Q. Structure prediction and functional analyses of a thermostable lipase obtained from Shewanella putrefaciens. *Journal of Biomolecular Structure and Dynamics.* **2017***,* 35, 2123-2135.

(20) Trott, O.; Olson, A. J. AutoDock Vina: Improving the speed and accuracy of docking with a new scoring function, efficient optimization, and multithreading. *Journal of Computational Chemistry.* **2010***,* 31, 455-461.

(21) Khan, S.; Khan, F. I.; Mohammad, T.; Khan, P.; Hasan,G. M.; Lobb, K. A.; Islam, A.; Ahmad, F.; Hassan, M. I. Exploring molecular insights into the interaction mechanism of cholesterol derivatives with the Mce4A: A combined spectroscopic and molecular dynamic simulation studies. *International Journal of Biological Macromolecules.* **2018,** 111, 548-560.

(22) Naz, F.; Khan, F. I.; Mohammad, T.; Khan, P.; Manzoor, S.; Hasan, G. M.; Lobb, K. A.; Luqman, S.; Islam, S.; Ahmad, F.; Hassan, M. I. Investigation of molecular mechanism of recognition between citral and MARK4: A newer therapeutic approach to attenuate cancer cell progression. *International Journal of Biological Macromolecules.* **2018***,* 107, 2580-2589.

(23) Rigsby, R. E.; Parker, A. B. Using the PyMOL application to reinforce visual understanding of protein structure. *Biochemistry and Molecular Biology Education.* **2016***,* 44, 433-437.

(24) Discovery studio modeling environment. San Diego: Dassault Systemes (San Diego, 2015)

(25) Laskowski, R. A.; Swindells, M. B. LigPlot+: Multiple Ligand–Protein Interaction Diagrams for Drug Discovery. *Journal of Chemical Information and Modeling.* **2011***,* 51, 2778-2786.

(26) Link, S.; El-Sayed, M. A. Optical Properties and Ultrafast Dynamics of Metallic Nanocrystals. *Annual Review of Physical Chemistry.***2003***,* **54**, 331-366.

(27) Cho, W. S.; Thielbeer, F.; Duffin, R,; Johansson, E. M. V.; Megson, I. L.; MacNee, W.; Bradley, M.; Donaldson, K. Surface functionalization affects the zeta potential, coronal stability and membranolytic activity of polymeric nanoparticles. *Nanotoxicology.***2014***,* 8, 202-211.

(28) Jack L. A.; Baskaran G.; Traci E. B.; Rebecca L.; David A. F.; Masuko U. F.; Betsy N. P.; David F. S.; Tim Bowden G.; Anquan L.; Eva K.; Pawel J. K.; Tony Eissa N.; Chowdhury F. H.; Dale G. N. Carbazole Is a Naturally Occurring Inhibitor of Angiogenesis and Inflammation Isolated from Antipsoriatic Coal Tar. *Journal of Investigative Dermatology*, **2006**, 126, 6, 1396-1402.

(29) Moonsamy, S.; Bhakat, S.; Ramesh, M.; Soliman, M. E. Identification of Binding Mode and Prospective Structural Features of Novel Nef Protein Inhibitors as Potential Anti-HIV Drugs. *Cell Biochem Biophys*. **2017**, 75, 49-64.

(30) Ramesh, M.; Bharatam, P. V. Importance of hydrophobic parameters in identifying appropriate pose of CYP substrates in cytochromes. *Eur. J. Med. Chem*. **2014**, 71, 15-23.

(31) Morris, G. M.; Lim-Wilby, M. Molecular docking. *Methods Mol Biol*. **2008**, 443, 365-82. 636-650.

(32) Debnath, S.; Kanakaraju, M.; Islam, M.; Yeeravalli, R.; Sen, D.; Das, A. In silico design, synthesis and activity of potential drug-like chrysin scaffold-derived selective EGFR inhibitors as anticancer agents. *Comput. Biol. Chem*. **2019**, 83, 107156.

(33) Cele, F.N.; Ramesh, M.; Soliman, M. E. Per-residue energy decomposition pharmacophore model to enhance virtual screening in drug discovery: a study for identification of reverse transcriptase inhibitors as potential anti-HIV agents. *Drug. Des. Devel. Ther.* **2016**, 10, 1365-77.

(34) Pettersen, E. F.; Goddard, T. D.; Huang, C.C.; Couch, G. S.; Greenblatt, D. M.; Meng, E. C.; Ferrin, T. E. UCSF Chimera--a visualization system for exploratory research and analysis. *J. Comput. Chem*. **2004**, 13, 1605-12.

(35) Todorov, I. T.; Smith, W. DL_POLY_3: the CCP5 national UK code for molecular-dynamics simulations. Philos. Trans. *A Math Phys Eng Sci*. **2004**, 362, 1835-52.

(36) Jorgensen, W. L.; Chandrasekhar, J.; Madura, J. D. Comparison of simple potential functions for simulating liquid water. The *J. Chem. Phys.* **1983**, 79, 926-935.

(37) Berendsen, H. J. C.; Postma, J. P. M.; van Gunsteren, W. F.; DiNola, A.; Haak, J. R. Molecular dynamics with coupling to an external bath. *J. Chem. Phys*. **1984**, 81, 3684–3690.

(38) Roe, D. R.; Cheatham, T. E.; PTRAJ and CPPTRAJ: Software for Processing and Analysis of Molecular Dynamics Trajectory Data. *J. Chem. Theory Comput*. **2013**, 9, 3084–3095.

List of Figure Captions

Figure 1 The literature reported amphiphilic Drug–Drug conjugate for cancer therapy

Figure 2 Synthesis of Carbazole Thiooctanoic acid (CT) [3] and Plausible ‘’Amine to Amide’’ mechanism for the formation of CT

Figure 3 Schematic route for the formation of amphiphilic twin bioactive molecule and its self-assembly for endocytosis.

Figure 4 Morphology of amphiphilic CT nanoparticles

Figure 5 DLS profile: size distribution of CTN nanoparticles with PDI:0.041

Figure 6 The outline for the synthesis of CT capped gold nanoparticles (CTAuNPs)

Figure 7 UV–vis spectra of gold nanoparticles line (a) (red color) and CTN capped gold nanoparticles line (b) (blue color)

Figure 8 HRTEM images of (A) Before CTN capped gold nanoparticles (B) After adding CTN gold nanoparticles in solution (C) HRTEM image of a part of spherical gold nanoparticle and its corresponding fast Fourier transformed image

Figure 9 (A) Particle size distribution of CTAuNPs by DLS method (B) Zeta potential measurement by Zeta sizer

Figure 10 The FTIR Profile of CT (line A) and CTAuNPs (line B).

Figure 11 MTT evaluation of cell viability for CTN (A) and CTAuNPs (B) in HepG2 cells.

Figure 12 Schematic representation of CTN induced apoptosis.

Figure 13 (A) CTN increased the activity of the extrinsic caspase 8, (B) intrinsic caspase 9 and (C) executioner caspases 3/7. Key: *** $p<0.001$ $p<0.05$

Figure 14 Effect of CTN on ATP detection

Figure 15 Effect of CTN on LDH leakage

Figure 16 The interaction pattern of CT with EGFR in molecular docking

Figure 17. The binding landscape of CT inside the ligand binding site of EGFR in molecular docking

Figure 18. (A) RMSD and (B) RMSF plots of the carbazole-thiooctanoic acid (CT) with EGFR complex in molecular dynamics simulation

List of Table Captions

Table 1. Molecular docking scores of the molecules (Aminocarbazole, Lipoic acid, and CT)

Table 2. The energy components of CT-EGFR complex in molecular dynamics simulation